

Two-point functions and the vacuum densities in the Casimir effect for the Proca field

A. A. Saharian* and H. H. Asatryan
*Institute of Physics, Yerevan State University,
1 Alex Manoogian Street, 0025 Yerevan, Armenia*

July 11, 2025

Abstract

We investigate the properties of the vacuum state for the Proca field in the geometry of two parallel plates on background of $(D+1)$ -dimensional Minkowski spacetime. The two-point functions for the vector potential and the field tensor are evaluated for higher-dimensional generalizations of the perfect magnetic conductor (PMC) and perfect electric conductor (PEC) boundary conditions. Explicit expressions are provided for the vacuum expectation values (VEVs) of the electric and magnetic field squares, field condensate, and for the VEV of the energy-momentum tensor. In the zero-mass limit the VEVs of the electric and magnetic field squares and the condensate reduce to the corresponding expressions for a massless vector field. The same is the case for the VEV of the energy-momentum tensor in the problem with PEC conditions. However, for PMC conditions the zero-mass limit for the vacuum energy-momentum tensor differs from the corresponding VEV for a massless field. This difference in the zero-mass limits is related to the different influences of the boundary conditions on the longitudinal polarization mode of a massive vector field. The PMC conditions constrain all the polarization modes including the longitudinal mode, whereas PEC conditions do not influence the longitudinal mode. The vacuum energy-momentum tensor is diagonal. The normal stress is uniformly distributed in the region between the plates and vanishes in the remaining regions. The corresponding Casimir forces are attractive for both boundary conditions. The Casimir-Polder forces acting on a polarizable particle are repulsive with respect to the nearest plate for PMC conditions. For PEC conditions those forces are attractive for $D \geq 2$ and vanish for $D = 1$. For $D \geq 3$, the vacuum energy density is positive for the PMC conditions and negative for the PEC conditions. For $D = 2$ and for PMC conditions, the vacuum energy density is negative in the region between the plates and vanishes in the remaining regions. For $D = 1$ and PMC conditions, the energy density is negative everywhere. In the case of PEC conditions, the vacuum energy density is positive for $D = 2$ and vanishes for $D = 1$.

Keywords: Casimir effect, Proca field, perfect conductor boundary conditions

1 Introduction

In several problems in quantum field theory, the interaction of a field with external stimuli can be described by an effective model, in which boundary or periodicity conditions are imposed on the field operator. These conditions affect the spectrum of quantum fluctuations of the field, resulting in changes to the expectation values of the physical observables that characterize the given state. The dependence of physical quantities on specified conditions is known by the general name Casimir effect (for reviews see [1, 2, 3, 4]). This effect has been investigated for various fields, boundary conditions, boundary and

*Corresponding author, E-mail: saharian@ysu.am

background geometries. The great interest in the Casimir effect is due to its important role in condensed matter physics, quantum field theory, gravitation, and cosmology.

In the literature, the Casimir effect has been studied for fields with different spins. This has been done for both massless and massive fields. In the case of massive fields, the expectation values of physical quantities associated with the Casimir effect typically decay exponentially when the distance of the observation point from the boundary exceeds the Compton wavelength. However, in background gravitational fields, the behavior at large distances can exhibit qualitative differences. Such behavior is present, for example, in the Casimir effect on the background of de Sitter spacetime [5, 6, 7]. The decay of the vacuum densities for both planar and spherical boundaries, as functions of the distance from the boundary, is the power law for both massless and massive fields. Depending on the value of the field mass, the fall-off can be monotonic or damping oscillatory.

Motivated by applications in electromagnetism, the Casimir effect for vector fields has been studied mainly for the massless case. However, massive vector fields appear in a number of physical models. Of particular relevance are the gauge vector fields within the Standard Model. In electrodynamic systems, a photon can also acquire an effective mass, and the corresponding dynamics can be described in terms of a massive vector field model. These include electrodynamic models in media and theories with extra dimensions. The motivation to investigate quantum phenomena in the context of massive vector fields is also attributed to the potential non-zero mass of the photon (for constraints on the photon mass see, e.g., [8, 9]). Two approaches have been discussed in the literature to introduce the mass for vector fields. In the first one, the term $m^2 A_\mu A^\mu$ is added to the Maxwellian Lagrangian for the electromagnetic field with the vector potential A_μ . This term breaks the local gauge invariance of the theory. The corresponding field is known in the literature as the Proca vector field (sometimes also as the de Broglie-Proca field) [10]. In the second approach, suggested in [11, 12] (for a review see [13]), in addition to the mass term an additional scalar field φ is introduced in the Lagrangian density, directly interacting with the vector field through the term $-mA^\mu \partial_\mu \varphi$. The gauge transformation of the scalar field φ compensates the gauge breaking part coming from the mass term $m^2 A_\mu A^\mu$ and the local gauge invariance is preserved. The corresponding theory is referred to as Stueckelberg massive electromagnetism. Note that the Stueckelberg Lagrangian is obtained from the Lagrangian for the Proca field by the replacement $A_\mu \rightarrow A_\mu + \partial_\mu \varphi / (\sqrt{2}m)$.

The nonzero mass of the vector field will give two types of modifications in the expressions for physical characteristics in the Casimir effect. The first one comes from the additional longitudinal polarization state and the second one is the modification in the contribution from transverse polarizations. Two possibilities in the standard Casimir setup for two parallel plates have been discussed in [14]. They correspond to complete reflection and perfect transmission for the modes of longitudinal polarization. More general problems with finite-width dielectric plates have been discussed in [15]. The Proca field modes and corresponding boundary conditions on the separation boundaries are presented in detail. The generalization for magnetodielectric plates at zero and finite temperatures is discussed in [16, 17]. The Casimir energy for a massive vector field in the geometry of perfectly conducting concentric spherical bodies is studied in [18]. The Casimir-Polder interactions with massive photons have been investigated in [19]. In models of extra compact spatial dimensions, the effective dynamics of 4D vector field is described in terms of the Proca Lagrangian with the mass determined by the length of compact dimensions. The Casimir effect in a simple 5D model with the extra dimension compactified to a circle is considered in [20]. The model with extra dimension of the Randall-Sundrum type has been discussed in [21]. The Casimir effect for Stueckelberg massive vector field is studied in [22]. Note that the precise measurements of the Casimir forces provide sensitive tests of new physics beyond the Standard Model (see, e.g., [3, 23, 24, 25] and references therein).

Previous research on the Casimir effect for the Proca field has focused on global characteristics of the vacuum in 3D space, such as the total vacuum energy and the forces acting on the boundaries with electric type conditions. Models with an extra dimension ($D = 4$) have also been considered incorporating 3D and 4D boundary conditions on planar boundaries. In the present paper, the local characteristics of the vacuum state for the geometry of parallel plates in a general number of spatial dimensions D

are investigated. Two types of boundary conditions are discussed, which generalize the $D = 3$ perfect magnetic conductor (PMC) and perfect electric conductor (PEC) boundary conditions to the general case of spatial dimension. The expectation values of local physical observables, bilinear in the field, are obtained from the two-point functions and their derivatives in the coincidence limit of the spacetime arguments. These functions will be evaluated for both types of boundary conditions.

The paper is organized as follows. In the next section, we describe the problem setup and present the mode functions for a massive Proca field obeying the PMC conditions on two parallel plates in a general number of spatial dimensions. The two-point Wightman functions for the vector potential and field tensor are considered in Section 3. By using these functions, the VEVs of local physical observables are investigated in Section 4. Aiming to compare the VEVs in the zero-mass limit of the Proca field with the corresponding VEVs for a massless vector field, the two-point functions and the expectation values for the latter are discussed in Section 5. The Casimir densities in the geometry of parallel plates for the Proca field with PEC conditions are investigated in Section 6. The main results of the paper are summarized in section 7. The details of the intermediate evaluation of the two-point functions are described in Appendix A.

2 Proca field modes for PMC boundary conditions

We consider massive Proca vector field $A_\mu(x)$ in $(D+1)$ -dimensional flat spacetime with the metric tensor $g_{\mu\nu} = \text{diag}(1, -1, \dots, -1)$ and the coordinates $(x^0 = t, x^1, \dots, x^{D-1}, x^D = z)$. The corresponding action is given by

$$S = \int d^{D+1}x L(A_\mu), \quad L(A_\mu) = -\frac{F_{\mu\nu}F^{\mu\nu} - 2m^2 A_\mu A^\mu}{16\pi}, \quad (2.1)$$

where $F_{\mu\nu} = \partial_\mu A_\nu - \partial_\nu A_\mu$ is the field tensor. The variation of the action with respect to the vector field leads to the field equation

$$\nabla_\nu F^{\mu\nu} - m^2 A^\mu = 0. \quad (2.2)$$

By taking into account that for an antisymmetric tensor $B^{\mu\nu}$ one has $\nabla_\mu \nabla_\nu B^{\mu\nu} = 0$, from (2.2) it follows that $m^2 \nabla_\mu A^\mu = 0$. Therefore, for a massive field ($m \neq 0$) we have

$$\partial_\mu A^\mu = 0. \quad (2.3)$$

For a massless field this is a gauge condition on the vector potential that is independent from the field equation. Substituting in (2.2) the expression for the field tensor one obtains the field equation in terms of the vector potential:

$$(\nabla_\nu \nabla^\nu + m^2) A^\mu = 0. \quad (2.4)$$

We are interested in the influence of two parallel plates, located at $z = 0$ and $z = a$, on the local properties of the vacuum state for the field $A_\mu(x)$. In this section, we assume that on the plates the field obeys the boundary condition

$$n^\nu F_{\mu\nu} = 0, \quad z = 0, a, \quad (2.5)$$

where $n^\nu = \delta_D^\nu$ is the normal to the plates. The boundary condition (2.5) is a higher dimensional generalization of PMC boundary conditions in Maxwell's electromagnetism (for the realization of PMC boundary conditions by using metamaterials see, for example, [26]). In terms of the $D = 3$ electric and magnetic fields \mathbf{E} and \mathbf{B} , they are written in the form $\mathbf{n} \cdot \mathbf{E} = 0$ and $\mathbf{n} \times \mathbf{B} = 0$. The condition (2.5) is also used in bag models for hadrons for confining the vector fields in finite regions. The properties of the vacuum state are encoded in two-point functions and for evaluation of those functions we will employ a direct summation over the complete set of vector modes obeying the boundary condition (2.5). The plates at $z = 0$ and $z = a$ divide the space into three spatial regions: $z < 0$, $0 < z < a$, and $z > a$. The following discussion will mainly concern the region between the plates. The two-point functions and

the expectation values in other regions are obtained by the limiting transition $a \rightarrow \infty$ while keeping the position of one of the plates fixed.

By taking into account the problem symmetry, we present the modes for the vector field in the form

$$A_\mu = f_\mu(z) e^{-ik_l x_\parallel^l}, \quad (2.6)$$

with the components of the wave vector k_l and $x_\parallel^l = (x^0, x^1, \dots, x^{D-1})$. Here and below, the latin indices take the values $l = 0, 1, \dots, D-1$. From the field equation (2.2) with $\mu = D$ it follows that

$$ik_l \partial_D f^l + k_D^2 f^D = 0, \quad (2.7)$$

where

$$k_D^2 = k_l k^l - m^2 = \omega^2 - \mathbf{k}^2 - m^2, \quad \omega = k^0, \quad \mathbf{k} = (k^1, k^2, \dots, k^{D-1}). \quad (2.8)$$

The equation (2.3) gives the relation

$$k_l f^l = -i \partial_z f^D. \quad (2.9)$$

Plugging this in (2.7) one obtains $\partial_z^2 f^D + k_D^2 f^D = 0$ with the general solution

$$f^D(z) = c_1^D e^{ik^D z} + c_2^D e^{-ik^D z}. \quad (2.10)$$

The field equation (2.2) with $\mu = l$, by taking into account (2.9), leads to the equation $\partial_z^2 f^l + k_D^2 f^l = 0$, having the general solution

$$f^l(z) = c_1^l e^{ik^D z} + c_2^l e^{-ik^D z}, \quad l = 0, 1, \dots, D-1. \quad (2.11)$$

The coefficients in (2.10) and (2.11) are connected by the relation (2.9):

$$k_l c_1^l = k^D c_1^D, \quad k_l c_2^l = -k^D c_2^D. \quad (2.12)$$

For the field tensor corresponding to the solutions of the form (2.6) one has

$$\begin{aligned} F^{nl} &= i \left(k^l f^n - k^n f^l \right) e^{-ik_l x_\parallel^l}, \\ F^{Dl} &= \left(-\partial_z f^l + i k^l f^D \right) e^{-ik_l x_\parallel^l}. \end{aligned} \quad (2.13)$$

The boundary condition (2.5) is reduced to the relations

$$\left(k^l c_1^D - k^D c_1^l \right) e^{ik^D z} + \left(k^l c_2^D + k^D c_2^l \right) e^{-ik^D z} = 0, \quad z = 0, a. \quad (2.14)$$

There are two classes of modes. The first one corresponds to transverse modes with $c_1^D = c_2^D = 0$ and $k_l c_1^l = k_l c_2^l = 0$. For them from (2.14) we find $c_1^l = c_2^l$. The corresponding eigenvalues for k^D are the roots of the equation $\sin(k^D a) = 0$ and they are given by $k^D = \pi n/a$ with $n = 1, 2, \dots$. The second class of modes corresponds to the longitudinal mode with $f^D \neq 0$. For it, multiplying (2.14) by k_l , summing over l , and by taking into account the relations (2.12), we get

$$m^2 \left(c_1^D e^{ik^D z} + c_2^D e^{-ik^D z} \right) = 0, \quad z = 0, a.$$

From here we see that $c_2^D = -c_1^D$ and, again, the eigenvalues are roots of the equation $\sin(k^D a) = 0$ with $k^D = \pi n/a$, $n = 1, 2, \dots$. In addition, there is also a zero mode with $k^D = 0$. For this mode, as it follows from (2.14), $f^D(z) = 0$.

The complete set of the vector modes is specified by the set of quantum numbers $\beta = (\mathbf{k}, k^D = \pi n/a, \sigma)$, where $\sigma = 1, 2, \dots, D$ enumerates the polarization degrees of freedom. Introducing the polarization vector $\epsilon_{(\sigma)}^l$, from the analysis given above it follows that for the transverse modes with polarizations $\sigma = 1, 2, \dots, D-1$ the corresponding vector potential is given by

$$A_{(\beta)l} = C_\beta \epsilon_{(\sigma)l} \cos(k^D z) e^{-ik_j x_{\parallel}^j}, \quad A_{(\beta)D} = 0. \quad (2.15)$$

For the polarization vector one has $k^l \epsilon_{(\sigma)l} = 0$ and

$$g^{il} \epsilon_{(\sigma')i} \epsilon_{(\sigma)l} = -\delta_{\sigma'\sigma}. \quad (2.16)$$

It obeys the relation

$$\sum_{\sigma=1}^{D-1} \epsilon_{(\sigma)i} \epsilon_{(\sigma)l} = \frac{k_i k_l}{\lambda^2} - g_{il}, \quad \lambda^2 = k_l k^l = k_D^2 + m^2. \quad (2.17)$$

In (2.15), the eigenvalues of k^D are given by

$$k^D = \frac{\pi n}{a}, \quad n = 0, 1, 2, \dots, \quad (2.18)$$

and they include also the zero mode with $n = 0$.

The longitudinal mode corresponds to the polarization $\sigma = D$ and for the corresponding vector potential one has

$$\begin{aligned} A_{(\beta)l} &= -\frac{k_l k^D}{\lambda^2} C_\beta \cos(k^D z) e^{-ik_j x_{\parallel}^j}, \\ A_{(\beta)D} &= i C_\beta \sin(k^D z) e^{-ik_j x_{\parallel}^j}, \end{aligned} \quad (2.19)$$

where the eigenvalues for k^D are given by (2.18) with $n = 1, 2, \dots$. Note that for this mode $F_{(\beta)ls} = \partial_l A_{(\beta)s} - \partial_s A_{(\beta)l} = 0$.

The vector modes are normalized by the condition

$$\int d^D x \left[A_{(\beta')\mu}^* \partial_0 A_{(\beta)}^\mu - \left(\partial_0 A_{(\beta')\mu}^* \right) A_{(\beta)}^\mu \right] = 4i\pi \delta_{\beta\beta'}, \quad (2.20)$$

which, for the modes (2.15) and (2.19) is reduced to

$$\int d^D x A_{(\beta')\mu}^* A_{(\beta)}^\mu = -\frac{2\pi}{\omega} \delta_{\beta\beta'}. \quad (2.21)$$

For the polarizations $\sigma = 1, 2, \dots, D-1$ this gives

$$|C_\beta|^2 = \frac{2(1 - \delta_{0n}/2)}{(2\pi)^{D-2} a \omega}, \quad (2.22)$$

and for the longitudinal polarization ($\sigma = D$):

$$|C_\beta|^2 = \frac{2\lambda^2}{(2\pi)^{D-2} m^2 a \omega}. \quad (2.23)$$

Note that for the latter the modes are singular in the zero mass limit.

3 Two-point functions for PMC conditions

In this section we consider the two-point functions for the vector potential and the field tensor.

3.1 Two-point functions for the vector potential

The two-point function for the vector potential (the positive-frequency Wightman function) is defined as the expectation value

$$\langle 0 | A_\mu(x) A_\nu(x') | 0 \rangle \equiv \langle A_\mu A'_\nu \rangle, \quad (3.1)$$

where $|0\rangle$ is the vacuum state. Having the complete set of modes $A_{(\beta)\mu}(x)$, it is evaluated by using the mode-sum formula

$$\langle A_\mu A'_\nu \rangle = \int d\mathbf{k} \sum_{\sigma=1}^D \sum_{n=0}^{\infty} A_{(\beta)\mu}(x) A_{(\beta)\nu}^*(x'). \quad (3.2)$$

The summation over the polarizations $\sigma = 1, 2, \dots, D-1$ is done by using the formula (2.17) and the components of the two-point functions are presented in the form

$$\begin{aligned} \langle A_\mu A'_\nu \rangle &= \left(\frac{\partial_\mu \partial'_\nu}{m^2} - g_{\mu\nu} \right) A(x, x'), \\ \langle A_D A'_D \rangle &= \frac{\partial_D \partial'_D}{m^2} A(x, x') + B(x, x'), \end{aligned} \quad (3.3)$$

where $\mu + \nu < 2D$. Here we have introduced the notations

$$\begin{aligned} A(x, x') &= \frac{2}{a} \int \frac{d\mathbf{k}}{(2\pi)^{D-2}} \sum_{n=0}^{\infty'} \frac{1}{\omega} \cos(k^D z) \cos(k^D z') e^{-ik_l \Delta x_\parallel^l}, \\ B(x, x') &= \frac{2}{a} \int \frac{d\mathbf{k}}{(2\pi)^{D-2}} \sum_{n=1}^{\infty} \frac{1}{\omega} \sin(k^D z) \sin(k^D z') e^{-ik_l \Delta x_\parallel^l}, \end{aligned} \quad (3.4)$$

where $\Delta x_\parallel^l = x_\parallel^l - x_\parallel'^l$ and the prime on the summation sign means that the term $n = 0$ should be taken with additional coefficient $1/2$. For the further transformation it is convenient to present the two-point functions (3.4) in the form

$$A(x, x') = \sum_{j=\mp 1} A_j(x, x'), \quad B(x, x') = - \sum_{j=\mp 1} j A_j(x, x'), \quad (3.5)$$

with the function

$$A_j(x, x') = \frac{1}{a} \int \frac{d\mathbf{k}}{(2\pi)^{D-2}} \sum_{n=0}^{\infty'} \frac{1}{\omega} \cos[k^D(z + jz')] e^{-ik_l \Delta x_\parallel^l}. \quad (3.6)$$

The representation (A.11) for this function, more convenient in the evaluation of the VEVs, is given in Appendix A. By using that representation, for the functions (3.4) we get

$$\begin{aligned} A(x, x') &= \frac{2m^{D-1}}{(2\pi)^{\frac{D-1}{2}}} \sum_{j=\mp 1} \sum_{n=-\infty}^{+\infty} f_{\frac{D-1}{2}}(mb_{j,n}(x, x')), \\ B(x, x') &= -\frac{2m^{D-1}}{(2\pi)^{\frac{D-1}{2}}} \sum_{j=\mp 1} \sum_{n=-\infty}^{+\infty} j f_{\frac{D-1}{2}}(mb_{j,n}(x, x')), \end{aligned} \quad (3.7)$$

where the notation

$$b_{j,n}(x, x') = \sqrt{(2na - z - jz')^2 - \Delta x_l \Delta x_l^l}, \quad (3.8)$$

is introduced. In (3.7), we have defined the function

$$f_\nu(x) = x^{-\nu} K_\nu(x), \quad (3.9)$$

with $K_\nu(x)$ being the modified Bessel function of the second kind.

Substituting (3.7) into (3.3) we find

$$\langle A_\mu A'_\nu \rangle = \frac{2m^{D-1}}{(2\pi)^{\frac{D-1}{2}}} \sum_{j=\mp 1} \sum_{n=-\infty}^{+\infty} A_{\mu\nu}^{(j,n)}(x, x'), \quad (3.10)$$

where

$$\begin{aligned} A_{il}^{(j,n)}(x, x') &= g_{il} D f_{\frac{D+1}{2}}(mb_{j,n}(x, x')) - m^2 (g_{il} b_{j,n}^2(x, x') + \Delta x_i \Delta x_l) f_{\frac{D+3}{2}}(mb_{j,n}(x, x')), \\ A_{Dl}^{(j,n)}(x, x') &= -m^2 (2na - z - jz') \Delta x_l f_{\frac{D+3}{2}}(mb_{j,n}(x, x')), \\ A_{DD}^{(j,n)}(x, x') &= j \left[D f_{\frac{D+1}{2}}(b_{j,n}(x, x')) + m^2 \Delta x_l \Delta x^l f_{\frac{D+3}{2}}(mb_{j,n}(x, x')) \right], \end{aligned} \quad (3.11)$$

and $A_{lD}^{(j,n)}(x, x') = -j A_{Dl}^{(j,n)}(x, x')$. In deriving these representations we have used the relation $f'_\nu(x) = -x f_{\nu+1}(x)$. Another relation for the function $f_\nu(x)$ directly follows from the recurrence relation for the modified Bessel function:

$$x^2 f_{\nu+1}(x) = 2\nu f_\nu(x) + f_{\nu-1}(x). \quad (3.12)$$

The two-point function (3.10) is decomposed into three contributions:

$$\langle A_\mu A'_\nu \rangle = \langle A_\mu A'_\nu \rangle_0 + \langle A_\mu A'_\nu \rangle_1 + \langle A_\mu A'_\nu \rangle_2, \quad (3.13)$$

where

$$\begin{aligned} \langle A_\mu A'_\nu \rangle_0 &= \frac{2m^{D-1}}{(2\pi)^{\frac{D-1}{2}}} A_{\mu\nu}^{(-1,0)}(x, x'), \\ \langle A_\mu A'_\nu \rangle_1 &= \frac{2m^{D-1}}{(2\pi)^{\frac{D-1}{2}}} A_{\mu\nu}^{(+1,0)}(x, x'), \\ \langle A_\mu A'_\nu \rangle_2 &= \frac{2m^{D-1}}{(2\pi)^{\frac{D-1}{2}}} \sum_{j=\mp 1} \sum_{n=-\infty, \neq 0}^{+\infty} A_{\mu\nu}^{(j,n)}(x, x'). \end{aligned} \quad (3.14)$$

The part $\langle A_\mu A'_\nu \rangle_0$ corresponds to the two-point function in the boundary-free geometry with $-\infty < z, z' < +\infty$. The sum of the two first terms in the right-hand side of (3.13) presents the two-point function in the region $z, z' > 0$ for the problem with a single plate at $z = 0$. Hence, the part $\langle A_\mu A'_\nu \rangle_1$ is interpreted as the contribution to the two-point function induced by the presence of a single plate at $z = 0$. Finally, the term $\langle A_\mu A'_\nu \rangle_2$ is induced by the second plate at $z = a$ when we add it to the geometry of a single plate at $z = 0$. Note that the part in (3.10) with $A_{\mu\nu}^{(+1,1)}(x, x')$ corresponds to the contribution of a single plate at $z = a$ (the plate at $z = 0$ is absent) in the region $z, z' < a$.

As it is seen from (3.10), the two-point functions of the vector potential are singular in the zero mass limit. In the expressions for the VEVs of physical observables the two-point functions enter in the form of the product $m^2 \langle A_\mu A'_\nu \rangle$. The zero mass limit of this product is finite and is given by

$$[m^2 \langle A_\mu A'_\nu \rangle]_{m \rightarrow 0} = \frac{2\Gamma(\frac{D+1}{2})}{\pi^{\frac{D-1}{2}}} \sum_{j=\mp 1} \sum_{n=-\infty}^{+\infty} \frac{A_{(0)\mu\nu}^{(j,n)}(x, x')}{b_{j,n}^{D+1}(x, x')}, \quad (3.15)$$

with the notations

$$\begin{aligned} A_{(0)il}^{(j,n)}(x, x') &= -g_{il} - (D+1) \frac{\Delta x_i \Delta x_l}{b_{j,n}^2(x, x')}, \\ A_{(0)Dl}^{(j,n)}(x, x') &= -(D+1) \Delta x_l \frac{2na - z - jz'}{b_{j,n}^2(x, x')}, \\ A_{(0)DD}^{(j,n)}(x, x') &= jD + j(D+1) \frac{\Delta x_l \Delta x^l}{b_{j,n}^2(x, x')}. \end{aligned} \quad (3.16)$$

The consequences for the nonzero zero-mass limit for physical observables bilinear in the field operator will be discussed below.

3.2 Two-point function for the field tensor

The VEVs of the electric and magnetic field squares are obtained from the two-point functions for the field tensor in the coincidence limit of the spacetime arguments. These two-point functions are defined as

$$\langle 0 | F_{\mu\nu}(x) F_{\rho\sigma}(x') | 0 \rangle = \langle F_{\mu\nu} F'_{\rho\sigma} \rangle, \quad (3.17)$$

with the expansion over the modes

$$\langle F_{\mu\nu} F'_{\rho\sigma} \rangle = \int d\mathbf{k} \sum_{\sigma=1}^D \sum_{n=0}^{\infty} F_{(\beta)\mu\nu}(x) F_{(\beta)\rho\sigma}^*(x'). \quad (3.18)$$

The mode functions have the form

$$\begin{aligned} F_{(\beta)lp} &= -iC_{\beta} (k_l \epsilon_{(\sigma)p} - k_p \epsilon_{(\sigma)l}) \cos(k^D z) e^{-ik_l x_{\parallel}^l}, \\ F_{(\beta)Dl} &= -C_{\beta} k^D \epsilon_{(\sigma)l} \sin(k^D z) e^{-ik_l x_{\parallel}^l}, \end{aligned} \quad (3.19)$$

for the polarizations $\sigma = 1, 2, \dots, D-1$ and

$$F_{(\beta)il} = 0, \quad F_{(\beta)Dl} = -C_{\beta} m^2 \frac{k_l}{\lambda^2} \sin(k^D z) e^{-ik_j x_{\parallel}^j}, \quad (3.20)$$

for the polarization $\sigma = D$. The normalization constants are given by (2.22) and (2.23). Note that, unlike the mode functions for the vector potential, the mode functions for the field tensor are regular in the zero-mass limit. For the longitudinal polarization ($\sigma = D$) the electric field is directed along the axis x^D and it vanishes on the plates.

With the mode functions (3.19) and (3.20), from (3.18) the following expressions are obtained

$$\begin{aligned} \langle F_{ik} F'_{lp} \rangle &= 2 [g_{p[i} \partial_{k]} \partial'_l + g_{l[k} \partial_i] \partial'_p] A(x, x'), \\ \langle F_{Di} F'_{kl} \rangle &= 2 g_{i[k} \partial'_l] \partial_D A(x, x'), \\ \langle F_{Di} F'_{Dl} \rangle &= \partial_i \partial'_l B(x, x') - g_{il} \partial_D \partial'_D A(x, x'), \end{aligned} \quad (3.21)$$

in terms of the functions (3.7). Here the square brackets in the expressions of indices mean the antisymmetrization over the enclosed indices:

$$a_{[i} b_{k]} = \frac{1}{2} (a_i b_k - a_k b_i). \quad (3.22)$$

Note that the longitudinal modes contribute only to the two-point function $\langle F_{Di} F'_{Dl} \rangle$.

By using the representation (3.7) we get

$$\langle F_{\mu\nu} F'_{\rho\sigma} \rangle = -\frac{4m^{D+1}}{(2\pi)^{\frac{D-1}{2}}} \sum_{j=\mp 1} \sum_{n=-\infty}^{\infty} F_{\mu\nu\rho\sigma}^{(j,n)}(x, x'), \quad (3.23)$$

with the functions

$$\begin{aligned} F_{iklp}^{(j,n)}(x, x') &= 2g_{p[i} g_{k]l} f_{\frac{D+1}{2}}(mb_{j,n}(x, x')) \\ &\quad + m^2 [g_{p[i} \Delta x_{k]} \Delta x_l - g_{l[i} \Delta x_{k]} \Delta x_p] f_{\frac{D+3}{2}}(mb_{j,n}(x, x')), \\ F_{Dikl}^{(j,n)}(x, x') &= m^2 g_{i[k} \Delta x_{l]} (2na - z - jz') f_{\frac{D+3}{2}}(mb_{j,n}(x, x')), \\ F_{DiDl}^{(j,n)}(x, x') &= j \left\{ -g_{il} f_{\frac{D+1}{2}}(mb_{j,n}(x, x')) \right. \\ &\quad \left. + \frac{m^2}{2} [g_{il} (2na - z - jz')^2 - \Delta x_i \Delta x_l] f_{\frac{D+3}{2}}(mb_{j,n}(x, x')) \right\}. \end{aligned} \quad (3.24)$$

Similar to the two-point function for the vector potential, the two-point function (3.23) is decomposed into the contributions corresponding to the boundary-free geometry (the part with $F_{\mu\nu\rho\sigma}^{(-1,0)}(x, x')$), to the part induced by a single plate at $z = 0$ in the region $z, z' > 0$ (the part with $F_{\mu\nu\rho\sigma}^{(+1,0)}(x, x')$), and to the part induced by the plate at $z = a$ in the region $0 < z, z' < a$ when we add it to the geometry with a single plate at $z = 0$ (the remaining part in (3.23)).

From (3.23) it follows that the two-point function for the field tensor is finite in the zero-mass limit. It is given by the formula

$$\langle F_{\mu\nu} F'_{\rho\sigma} \rangle_{m \rightarrow 0} = -4 \frac{\Gamma\left(\frac{D+1}{2}\right)}{\pi^{\frac{D-1}{2}}} \sum_{j=\mp 1} \sum_{n=-\infty}^{\infty} \frac{F_{(0)\mu\nu\rho\sigma}^{(j,n)}(x, x')}{b_{j,n}^{D+1}(x, x')}, \quad (3.25)$$

where the functions

$$\begin{aligned} F_{(0)iklp}^{(j,n)}(x, x') &= 2g_{p[i}g_{k]l} + (D+1) \frac{g_{p[i}\Delta x_k]\Delta x_l - g_{l[i}\Delta x_k]\Delta x_p}{b_{j,n}^2(x, x')}, \\ F_{(0)Dikl}^{(j,n)}(x, x') &= (D+1) g_{i[k}\Delta x_{l]} \frac{2na - z - jz'}{b_{j,n}^{D+3}(x, x')}, \\ F_{(0)DiDl}^{(j,n)}(x, x') &= -jg_{il} + j \frac{D+1}{2} \frac{g_{il}(2na - z - jz')^2 - \Delta x_i \Delta x_l}{b_{j,n}^2(x, x')}, \end{aligned} \quad (3.26)$$

are introduced for the separate components.

4 VEVs of the field squares and energy-momentum tensor

4.1 General expressions

The VEVs of the observables bilinear in the field operator are obtained from the two-point functions given above in the coincidence limit $x' \rightarrow x$. This limit is divergent. For points away from boundaries the divergences come from the part in the two-point functions corresponding to the boundary-free geometry. The important advantage of the representations given above is that the boundary-free contribution (denoted by $\langle \dots \rangle_0$) is explicitly separated. The renormalized VEVs are obtained by subtracting from the two-point functions the parts presenting the boundary-free geometry and then taking the coincidence limit $x' \rightarrow x$. All of the VEVs discussed below are symmetric with respect to the hyperplane $z = a/2$. This feature is a direct consequence of the problem symmetry.

We start the consideration from the VEV of the electric field squared. The corresponding renormalized VEV is given by

$$\langle E^2 \rangle = -g^{\mu\nu} \lim_{x' \rightarrow x} [\langle F_{0\mu} F'_{0\nu} \rangle - \langle F_{0\mu} F'_{0\nu} \rangle_0]. \quad (4.1)$$

By taking into account the expressions (3.23), (3.24) and using the relation (3.12) for the two-point functions in the region $0 < z < a$, we get

$$\begin{aligned} \langle E^2 \rangle &= -\frac{2m^{D+1}}{(2\pi)^{\frac{D-1}{2}}} \left\{ 2 \sum_{n=1}^{\infty} \left[(D-1) f_{\frac{D+1}{2}}(2nma) - f_{\frac{D-1}{2}}(2nma) \right] \right. \\ &\quad \left. + \sum_{n=-\infty}^{\infty} \left[3(D-1) f_{\frac{D+1}{2}}(2mz_n) + f_{\frac{D-1}{2}}(2mz_n) \right] \right\}, \end{aligned} \quad (4.2)$$

with the notation

$$z_n = |z - na|. \quad (4.3)$$

The $n = 0$ term in (4.2) corresponds to the VEV of the electric field squared in the geometry with a single plate $z = 0$:

$$\langle E^2 \rangle_1 = -\frac{2m^{D+1}}{(2\pi)^{\frac{D-1}{2}}} \left[3(D-1) f_{\frac{D+1}{2}}(2m|z|) + f_{\frac{D-1}{2}}(2m|z|) \right]. \quad (4.4)$$

This expression is valid in both regions $z > 0$ and $z < 0$. The VEV (4.4) is negative. The expression for the electric field squared in the region $z > a$ is obtained from (4.4) by the replacement $z \rightarrow z - a$. By taking into account that the function $f_\nu(x)$ is monotonically decreasing with increasing x , it can be shown that

$$\sum_{n=-\infty}^{\infty} f_\nu(2mz_n) > 2 \sum_{n=1}^{\infty} f_\nu(2ma). \quad (4.5)$$

From here it follows that the VEV (4.2) is negative as well. Hence, the VEV of the electric field squared for the PMC conditions is negative everywhere.

Another important bilinear combination of the field is the invariant

$$\langle F_{\mu\nu} F^{\mu\nu} \rangle = g^{\mu\rho} g^{\nu\sigma} \lim_{x' \rightarrow x} \left[\langle F_{\mu\nu} F'_{\rho\sigma} \rangle - \langle F_{\mu\nu} F'_{\rho\sigma} \rangle_0 \right]. \quad (4.6)$$

This VEV is the analog of the gluon condensate in quantum chromodynamics. Combining the formulas for the separate components of the two-point functions for the field tensor, one finds

$$\begin{aligned} \langle F_{\mu\nu} F^{\mu\nu} \rangle = & \frac{4Dm^{D+1}}{(2\pi)^{\frac{D-1}{2}}} \left\{ -2 \sum_{n=1}^{\infty} f_{\frac{D-1}{2}}(2nma) \right. \\ & \left. + \sum_{n=-\infty}^{\infty} \left[2(D-1) f_{\frac{D+1}{2}}(2mz_n) + f_{\frac{D-1}{2}}(2mz_n) \right] \right\}. \end{aligned} \quad (4.7)$$

This VEV is positive. For the VEV of the Lagrangian density we get

$$\langle L(A_\mu) \rangle = -\frac{Dm^{D+1}}{(2\pi)^{\frac{D+1}{2}}} \sum_{n=-\infty}^{\infty} \left[D f_{\frac{D+1}{2}}(2mz_n) + f_{\frac{D-1}{2}}(2mz_n) \right]. \quad (4.8)$$

The VEVs $\langle F_{\mu\nu} F^{\mu\nu} \rangle$ and $\langle L(A_\mu) \rangle$ in the region $z < 0$ coincide with the corresponding terms with $n = 0$ in (4.7) and (4.8). The expressions in the region $z > a$ are obtained from those in $z < 0$ by the replacement $z \rightarrow z - a$.

The VEV of the magnetic field squared, $\langle B^2 \rangle$, is obtained from the relation

$$\langle B^2 \rangle = \langle E^2 \rangle + \frac{1}{2} \langle F_{\mu\nu} F^{\mu\nu} \rangle. \quad (4.9)$$

This leads to the formula

$$\begin{aligned} \langle B^2 \rangle = & -\frac{2(D-1)m^{D+1}}{(2\pi)^{\frac{D-1}{2}}} \left\{ 2 \sum_{n=1}^{\infty} \left[f_{\frac{D+1}{2}}(2nma) + f_{\frac{D-1}{2}}(2nma) \right] \right. \\ & \left. - \sum_{n=-\infty}^{\infty} \left[(2D-3) f_{\frac{D+1}{2}}(2mz_n) + f_{\frac{D-1}{2}}(2mz_n) \right] \right\}. \end{aligned} \quad (4.10)$$

In the geometry of a single plate at $z = 0$ we have

$$\langle B^2 \rangle_1 = \frac{2(D-1)m^{D+1}}{(2\pi)^{\frac{D-1}{2}}} \left[(2D-3) f_{\frac{D+1}{2}}(2m|z|) + f_{\frac{D-1}{2}}(2m|z|) \right]. \quad (4.11)$$

Note that the VEV of the magnetic field squared is zero for $D = 1$. The VEV in the region $z > a$ is obtained from (4.11) making the replacement $z \rightarrow z - a$. For $D \geq 2$ the VEV of the magnetic field squared in the regions $z < 0$ and $z > a$ is negative for PMC boundary conditions on the plate. The same is the case for the region $0 < z < a$. That can be easily seen from (4.10) by using the relation (4.5).

Now we turn to the VEV of the energy-momentum tensor. For the Proca field the corresponding operator is given by the expression

$$T_{\mu\nu} = -\frac{g^{\alpha\rho}F_{(\mu\alpha}F_{\nu)\rho} - m^2 A_{(\mu}A_{\nu)}}{4\pi} - g_{\mu\nu}L(A_\mu), \quad (4.12)$$

where the Lagrangian density is given by (2.1) and the brackets in the expression for indices mean the symmetrization over the enclosed indices. By using the expressions for the VEVs of the separate parts in (4.12), given above, we see that the VEVs of the off-diagonal components vanish. For the diagonal components we get (no summation over l)

$$\begin{aligned} \langle T_l^l \rangle &= \frac{m^{D+1}}{(2\pi)^{\frac{D+1}{2}}} \left\{ -2D \sum_{n=1}^{\infty} f_{\frac{D+1}{2}}(2nma) + (D-2) \right. \\ &\quad \times \left. \sum_{n=-\infty}^{\infty} \left[(D-1) f_{\frac{D+1}{2}}(2mz_n) + f_{\frac{D-1}{2}}(2mz_n) \right] \right\}, \\ \langle T_D^D \rangle &= \frac{2Dm^{D+1}}{(2\pi)^{\frac{D+1}{2}}} \sum_{n=1}^{\infty} \left[D f_{\frac{D+1}{2}}(2nma) + f_{\frac{D-1}{2}}(2nma) \right], \end{aligned} \quad (4.13)$$

where $l = 0, 1, \dots, D-1$. This relations show that the vacuum energy density ($l = 0$) is equal to the stresses along the directions parallel to the plates. Of course, this property is a consequence of the invariance of the problem with respect to the Lorentz boosts along the directions parallel to the plates. The vacuum energy density is negative for $D \leq 2$ and positive for $D \geq 3$. Note that for $D = 2$ the distribution of the vacuum energy density in the region between the plates is uniform. The normal stress $\langle T_D^D \rangle$ does not depend on the z -coordinate and it vanishes in the geometry of a single plate. This property could be directly obtained from the conservation equation $\partial_\nu \langle T^{\mu\nu} \rangle = 0$.

The components of the vacuum energy-momentum tensor in the geometry of a single plate at $z = 0$ are given by the $n = 0$ term in (4.13) (no summation over l):

$$\langle T_l^l \rangle_1 = \frac{(D-2)m^{D+1}}{(2\pi)^{\frac{D+1}{2}}} \left[(D-1) f_{\frac{D+1}{2}}(2m|z|) + f_{\frac{D-1}{2}}(2m|z|) \right], \quad (4.14)$$

for $l = 0, 1, \dots, D-1$, and $\langle T_D^D \rangle_1 = 0$. The corresponding energy density is negative for $D = 1$ and positive for $D \geq 3$. For $D = 2$ the vacuum energy-momentum tensor for PMC boundary conditions vanishes in the problem with a single plate. The parallel plates divide the space into three regions. In the regions $z < 0$ and $z > a$ the normal stress vanishes and the energy density and parallel stresses are given by (4.14) for $z < 0$. The expressions for the energy density and parallel stresses for the region $z > a$ are obtained from (4.14) by the replacement $z \rightarrow z - a$. In the region between the plates, $0 < z < a$, the VEVs are expressed by the formulas (4.13). In this region, the energy density is negative for $D = 1, 2$ and positive for $D \geq 3$. The Casimir force per unit surface of the plates (the Casimir pressure) is determined by the normal stress as $p_C = -\langle T_D^D \rangle$. It is zero in the regions $z < 0$ and $z > a$ and is negative for the region between the plates. This corresponds to the attractive Casimir force. Hence, similar to the standard electromagnetic Casimir effect for parallel conducting plates, the attractive Casimir force is a consequence of a negative vacuum pressure in the region $0 < z < a$.

4.2 Zero-mass limit of the VEVs

Let us consider the limit $m \rightarrow 0$ for the VEVs given above. By taking into account that

$$f_\nu(y) \approx \frac{2^{\nu-1}}{y^{2\nu}} \Gamma(\nu), \quad (4.15)$$

for $0 < y \ll 1$, the VEVs of the electric and magnetic field squares are presented in the form

$$\begin{aligned} \langle E^2 \rangle_{m \rightarrow 0} &= \frac{(1-D) \Gamma\left(\frac{D+1}{2}\right)}{(4\pi)^{\frac{D-1}{2}} a^{D+1}} \left[\zeta(D+1) + \sum_{n=-\infty}^{+\infty} \frac{3/2}{|n - z/a|^{D+1}} \right], \\ \langle B^2 \rangle_{m \rightarrow 0} &= \frac{(1-D) \Gamma\left(\frac{D+1}{2}\right)}{(4\pi)^{\frac{D-1}{2}} a^{D+1}} \left[\zeta(D+1) + \sum_{n=-\infty}^{+\infty} \frac{3/2 - D}{|n - z/a|^{D+1}} \right], \end{aligned} \quad (4.16)$$

where $\zeta(y) = \sum_{n=1}^{\infty} n^{-y}$ is the Riemann zeta function. For the condensate we get

$$\langle F_{\mu\nu} F^{\mu\nu} \rangle_{m \rightarrow 0} = \frac{2D \Gamma\left(\frac{D+1}{2}\right)}{(4\pi)^{\frac{D-1}{2}} a^{D+1}} \sum_{n=-\infty}^{+\infty} \frac{D-1}{|n - z/a|^{D+1}}. \quad (4.17)$$

The expressions for the nonzero components of the vacuum energy-momentum tensor in the zero-mass limit read (no summation over l)

$$\begin{aligned} \langle T_l^l \rangle_{m \rightarrow 0} &= \frac{D \Gamma\left(\frac{D+1}{2}\right)}{(4\pi)^{\frac{D+1}{2}} a^{D+1}} \left[\frac{D-2}{2D} \sum_{n=-\infty}^{\infty} \frac{D-1}{|n - z/a|^{D+1}} - \zeta(D+1) \right], \\ \langle T_D^D \rangle_{m \rightarrow 0} &= \frac{D^2 \Gamma\left(\frac{D+1}{2}\right)}{(4\pi)^{\frac{D+1}{2}} a^{D+1}} \zeta(D+1). \end{aligned} \quad (4.18)$$

For the corresponding trace one gets

$$\langle T_l^l \rangle_{m \rightarrow 0} = \frac{D \Gamma\left(\frac{D+1}{2}\right)}{2 (4\pi)^{\frac{D+1}{2}} a^{D+1}} \sum_{n=-\infty}^{\infty} \frac{(D-1)(D-2)}{|n - z/a|^{D+1}}. \quad (4.19)$$

The VEV of the energy-momentum tensor in the zero mass limit is traceless in spatial dimensions $D = 1, 2$. In spatial dimensions $D \geq 3$ the trace is nonzero. In the massless limit the action (2.1) is conformally invariant for $D = 3$ and the appearance of the nonzero trace (4.19) can be considered as a kind of trace anomaly. It is different from the standard trace anomaly induced by the curvature of the spacetime (see, e.g., [27]).

Figure 1 presents the dependence of the vacuum energy density for the Proca field (measured in units of $1/a^{D+1}$) in the limit $m \rightarrow 0$ (see (4.18)) as a function of z/a . The graphs are plotted for $D = 3, 4, 5, 6$. The product $a^{D+1} \langle T_0^0 \rangle_{m \rightarrow 0}$ increases with increasing D .

4.3 Asymptotic and numerical analysis

For points near the plate at $z = 0$, $|z|/a \ll 1$, the dominant contribution to the VEVs $\langle E^2 \rangle$, $\langle B^2 \rangle$, and to the vacuum energy density and parallel stresses comes from the terms $n = 0$ in (4.2), (4.10), and (4.13). The leading terms in the asymptotic expansions over $|z|/a$ coincide with the terms $n = 0$ in (4.16) and (4.18) (no summation over l):

$$\begin{aligned} \langle E^2 \rangle &\approx \frac{3 \langle B^2 \rangle}{3 - 2D} \approx -\frac{3(D-1) \Gamma\left(\frac{D+1}{2}\right)}{2 (4\pi)^{\frac{D-1}{2}} |z|^{D+1}}, \\ \langle T_l^l \rangle &\approx \frac{(D-2)(D-1) \Gamma\left(\frac{D+1}{2}\right)}{2 (4\pi)^{\frac{D+1}{2}} |z|^{D+1}}. \end{aligned} \quad (4.20)$$

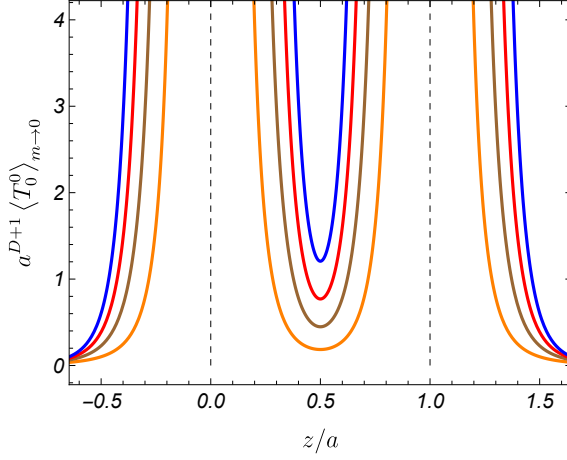


Figure 1: Vacuum energy density (in units $1/a^{D+1}$) as a function of z/a for the Proca field in the limit $m \rightarrow 0$. The graphs are plotted for $D = 3, 4, 5, 6$. The product $a^{D+1} \langle T_0^0 \rangle$ increases with increasing D .

The leading terms near the plate at $z = a$, assuming that $|z/a - 1| \ll 1$, are obtained from (4.20) making the replacement $|z| \rightarrow |z - a|$. In particular, the VEV of the electric field squared is negative near the plates and the energy density is positive for $D \geq 3$.

Figure 2 displays the VEVs of the electric ($U = E$, full curves) and magnetic ($U = B$, dashed curves) field squares (measured in units of m^{D+1}) for the Proca field in 3-dimensional space ($D = 3$) versus z/a . The graphs are plotted for $ma = 0.75, 1, 1.25, 1.5$. The VEVs $|\langle U^2 \rangle|/m^{D+1}$, with $U = E$ and $U = B$, are decreasing functions of ma .

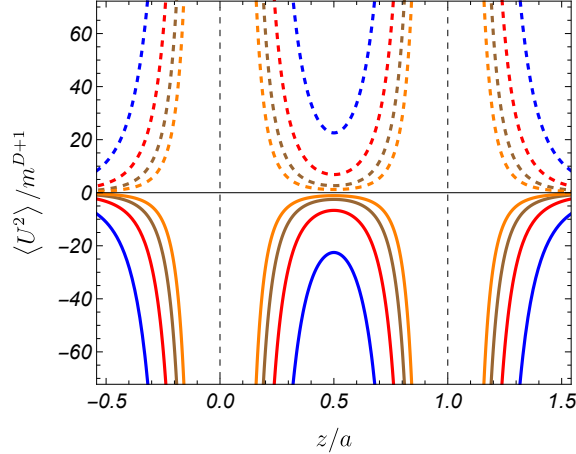


Figure 2: The VEVs of the electric ($U = E$, full curves) and magnetic ($U = B$, dashed curves) field squares (measured in units of m^{D+1}) as functions of z/a for the $D = 3$ Proca field. The graphs are plotted for $ma = 0.75, 1, 1.25, 1.5$. The ratio $|\langle U^2 \rangle|/m^{D+1}$ is a decreasing function of ma .

The VEV of the electric field squared determines the Casimir-Polder interaction energy between the plates and a polarizable particle. For an isotropic polarizability, neglecting the effects of dispersion, the potential is expressed as $U_{CP} = -\alpha_P \langle E^2 \rangle / 2$, where α_P is the static polarizability of the particle. From the analysis of the electric field squared given above it follows that for PMC conditions the Casimir-Polder force is repulsive with respect to the nearest plate.

In figure 3 we have plotted the energy density for the Proca field in 3-dimensional space ($D = 3$) as a function of z/a for $ma = 0.75, 1, 1.25, 1.5$. The ratio $\langle T_0^0 \rangle / m^{D+1}$ decreases with increasing ma .

For small separations between the plates, compared with the Compton wavelength, one has $ma \ll 1$.

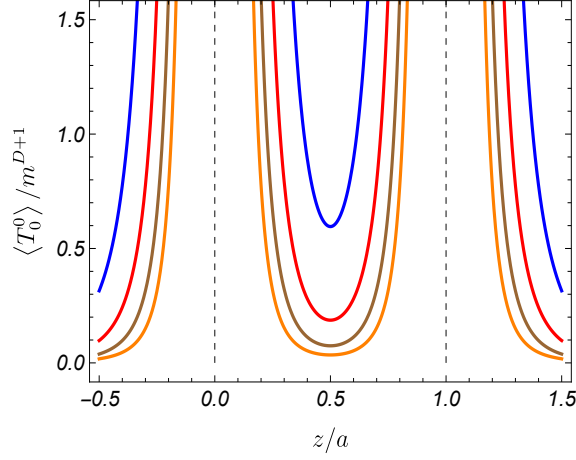


Figure 3: Vacuum energy density (in units of m^{D+1}) versus z/a for a massive vector field in $D = 3$ spatial dimensions. The graphs are plotted for $ma = 0.75, 1, 1.25, 1.5$. The ratio $\langle T_0^0 \rangle / m^{D+1}$ decreases with increasing ma .

By using the expansion of the function $f_\nu(y)$ for small argument, given in the previous subsection, for the leading term in the Casimir pressure we get

$$p_C \approx -\frac{D^2 \Gamma\left(\frac{D+1}{2}\right)}{(4\pi)^{\frac{D+1}{2}} a^{D+1}} \zeta(D+1). \quad (4.21)$$

This coincides with the result in the zero-mass limit. At large separations between the plates, $ma \gg 1$, the Casimir forces are exponentially suppressed:

$$p_C \approx -\frac{D(D+1)m^{D+1}}{(2\pi)^{\frac{D}{2}} \sqrt{2ma}} e^{-2ma}. \quad (4.22)$$

Figure 4 displays the Casimir pressure versus the distance between the plates (in units of the Compton wavelength) for different values of the spatial dimension D . The pressure is negative and corresponds to an attractive Casimir force.

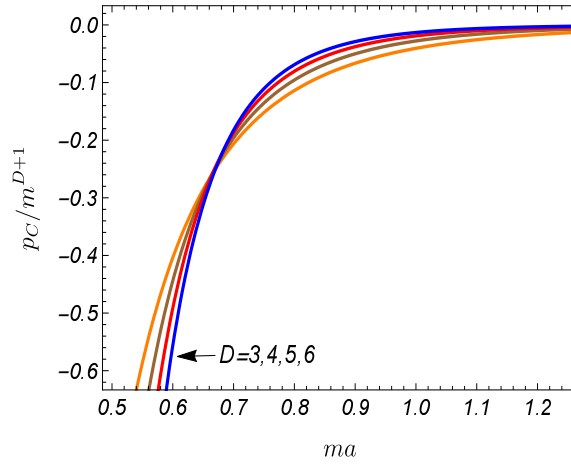


Figure 4: The Casimir pressure for PMC conditions as a function of the distance between the plates for $D = 3, 4, 5, 6$.

5 Two-point functions and the Casimir densities for a massless vector field with PMC conditions

In order to compare the zero-mass limit of the VEVs for Proca field with PMC boundary conditions, in this section we consider the two-point functions and the VEVs for a massless vector field. The total vacuum energy for PMC Casimir piston in $(D+1)$ -dimensional spacetime has been investigated in [28].

5.1 Modes and the two-point functions for the field tensor

The action for a massless vector field is invariant under the gauge transformation $A'_\mu(x) = A_\mu(x) + \partial_\mu \chi(x)$. Fixing the gauge by the conditions $\partial_\mu A^\mu(x) = 0$ and $A_D(x) = 0$, for the mode functions with $k_D \neq 0$ we have

$$A_{(\beta)l}^{(0)} = C_\beta \epsilon_{(\sigma)l}^{(0)} \cos(k^D z) e^{-ik_j x^j}, \quad A_{(\beta)D}^{(0)} = 0. \quad (5.1)$$

where

$$k^D = \frac{\pi n}{a}, \quad k^0 = \omega = \sqrt{|\mathbf{k}|^2 + (k^D)^2}, \quad n = 1, 2, \dots \quad (5.2)$$

In this case the longitudinal polarization is absent and $\sigma = 1, \dots, D-1$. As before, one has $k^l \epsilon_{(\sigma)l}^{(0)} = 0$, $g^{il} \epsilon_{(\sigma')i}^{(0)} \epsilon_{(\sigma)l}^{(0)} = -\delta_{\sigma'\sigma}$, and the relation

$$\sum_{\sigma=1}^{D-1} \epsilon_{(\sigma)i}^{(0)} \epsilon_{(\sigma)l}^{(0)} = \frac{k_i k_l}{k_D^2} - g_{il}. \quad (5.3)$$

The normalization coefficient C_β in (5.1) is given by (2.22) with $n \neq 0$ and ω from (5.2).

In addition, there are also zero modes with

$$A_{(0\beta)l}^{(0)} = C_\beta \epsilon_{(0\sigma)l}^{(0)} e^{-ik_j x^j}, \quad A_{(0\beta)D}^{(0)} = 0, \quad (5.4)$$

where $g_{il} k^i k^l = 0$ and $k^0 = \omega = |\mathbf{k}|$. In this case we have $D-2$ polarization degrees of freedom ($\sigma = 1, 2, \dots, D-2$) with $\epsilon_{(0\sigma)0}^{(0)} = 0$. The polarization vector obeys the relations

$$\epsilon_{(0\sigma)l}^{(0)} \epsilon_{(0\sigma')l}^{(0)} = -\delta_{\sigma\sigma'}, \quad \sum_{\sigma=1}^{D-2} \epsilon_{(0\sigma)i}^{(0)} \epsilon_{(0\sigma)l}^{(0)} = -\frac{k_i k_l}{|\mathbf{k}|^2} - g_{il}, \quad (5.5)$$

where $i, l = 1, 2, \dots, D-1$. The coefficient C_β in (5.4) is obtained from (2.22) with $n = 0$ and $\omega = |\mathbf{k}|$.

By using the mode functions (5.1) and (5.4), for the two-point functions of the field tensor in the region between the plates we get

$$\begin{aligned} \langle F_{\mu\nu} F'_{\rho\sigma} \rangle^{(0)} &= 2 (\eta_{[\mu\sigma} \partial_{\nu]} \partial'_\rho - \eta_{[\mu\rho} \partial_{\nu]} \partial'_\sigma) A_0(x, x'), \\ \langle F_{D\mu} F'_{D\nu} \rangle^{(0)} &= \partial_\mu \partial'_\nu B_0(x, x') - \eta_{\mu\nu} \partial_D \partial'_D A_0(x, x'), \end{aligned} \quad (5.6)$$

where the functions $A_0(x, x')$ and $B_0(x, x')$ are defined by (3.4) with $m = 0$. We note that the contribution of the term $n = 0$ in $A_0(x, x')$ comes from the zero modes (5.4). Simpler expressions for the functions $A_0(x, x')$ and $B_0(x, x')$ are obtained from (3.7) in the limit $m \rightarrow 0$:

$$\begin{aligned} A_0(x, x') &= \frac{\Gamma(\frac{D-1}{2})}{\pi^{\frac{D-1}{2}}} \sum_{j=\mp 1} \sum_{n=-\infty}^{+\infty} \frac{1}{b_{j,n}^{D-1}(x, x')}, \\ B_0(x, x') &= -\frac{\Gamma(\frac{D-1}{2})}{\pi^{\frac{D-1}{2}}} \sum_{j=\mp 1} \sum_{n=-\infty}^{+\infty} \frac{j}{b_{j,n}^{D-1}(x, x')}. \end{aligned} \quad (5.7)$$

Evaluating the derivatives, we get

$$\langle F_{\mu\nu} F'_{\rho\sigma} \rangle^{(0)} = \langle F_{\mu\nu} F'_{\rho\sigma} \rangle_{m \rightarrow 0}, \quad (5.8)$$

and the two-point function of the field tensor for a massless vector field coincides with the zero-mass limit of the corresponding function for a massive vector field, given by (3.25).

5.2 VEVs and the Casimir forces

Given the two-point functions for the field tensor we can evaluate the VEVs of physical observables. By taking into account the relation (5.8), we conclude that the VEVs of the electric and magnetic field squares and the condensate coincide with the corresponding VEVs of the massive field in the zero-mass limit:

$$\langle E^2 \rangle^{(0)} = \langle E^2 \rangle_{m \rightarrow 0}, \quad \langle B^2 \rangle^{(0)} = \langle B^2 \rangle_{m \rightarrow 0}, \quad (5.9)$$

and $\langle F_{\mu\nu} F^{\mu\nu} \rangle^{(0)} = \langle F_{\mu\nu} F^{\mu\nu} \rangle_{m \rightarrow 0}$. The corresponding expressions are given by (4.16) and (4.17). By using the mode functions (5.1) and (5.4), for the nonzero components of the vacuum energy-momentum tensor we find (no summation over l)

$$\begin{aligned} \langle T_l^l \rangle^{(0)} &= \frac{(1-D) \Gamma(\frac{D+1}{2})}{(4\pi)^{\frac{D+1}{2}} a^{D+1}} \left[\zeta(D+1) - \sum_{n=-\infty}^{+\infty} \frac{(D-3)/2}{|n-z/a|^{D+1}} \right], \\ \langle T_D^D \rangle^{(0)} &= \frac{D(D-1) \Gamma(\frac{D+1}{2})}{(4\pi)^{\frac{D+1}{2}} a^{D+1}} \zeta(D+1), \end{aligned} \quad (5.10)$$

with $l = 0, 1, \dots, D-1$. For $D = 3$ the massless vector field is conformally invariant and the vacuum energy-momentum tensor is traceless: $\langle T_\mu^\mu \rangle^{(0)} = 0$. Comparing the VEVs (4.18) and (5.10), we see that they are different: $\langle T_{\mu\nu} \rangle_{m \rightarrow 0} \neq \langle T_{\mu\nu} \rangle^{(0)}$. The Casimir densities for a massless vector field in the geometry of two parallel plates on the background of $(D+1)$ -dimensional anti-de Sitter (AdS) spacetime (the plates are parallel to the AdS boundary) were investigated in [29] for both PMC and PEC boundary conditions (for the electromagnetic Casimir densities in the geometry of planar boundaries in de Sitter spacetime see [30, 31]). As it has been shown in [29], the VEVs $\langle E^2 \rangle^{(0)}$, $\langle B^2 \rangle^{(0)}$, and $\langle T_\mu^\nu \rangle^{(0)}$ are obtained from the results for the AdS bulk in the limit when the curvature radius goes to infinity.

For a massive field, the VEV of the energy-momentum tensor, in addition to the terms with the expectation values of the products of the field tensor, contains the terms with the products of the vector potential multiplied by the mass squared. As it has been discussed above, the zero-mass limit of those parts does not vanish. As a consequence, the VEV of the energy-momentum tensor for a massless field differs from the corresponding VEV for a massive field in the zero-mass limit. We have the following relation

$$\langle T_{\mu\nu} \rangle_{m \rightarrow 0} = \langle T_{\mu\nu} \rangle^{(0)} + \lim_{m \rightarrow 0} \frac{m^2}{4\pi} \left(\langle A_{(\mu} A_{\nu)} \rangle - \frac{1}{2} g_{\mu\nu} \langle A_\alpha A^\alpha \rangle \right), \quad (5.11)$$

for the corresponding VEVs. This relation is easy to check by using the expression (3.15) for the zero-mass limit of the VEVs bilinear in the vector field.

6 The Casimir densities for PEC conditions

In this section, we consider the two-point functions and the Casimir densities for the boundary condition being the higher dimensional generalization of the condition imposed on the surface of perfect conductor in spatial dimensions $D = 3$ (PEC boundary condition). In terms of the dual tensor ${}^*F_{\mu_1 \dots \mu_{D-1}} = \varepsilon_{\mu\nu\mu_1 \dots \mu_{D-1}} F^{\mu\nu} / (D-1)!$, with $\varepsilon_{\mu\nu\mu_1 \dots \mu_{D-1}}$ being the Levi-Civita tensor, the boundary conditions are written as

$$n^{\mu_1} {}^*F_{\mu_1 \dots \mu_{D-1}} = 0, \quad z = 0, a. \quad (6.1)$$

In the geometry under consideration they are reduced to $F_{il} = 0$ for $z = 0, a$, and $i, l = 0, 1, \dots, D-1$.

6.1 Mode functions

Similar to the case of PMC boundary conditions, we have $D-1$ transverse polarizations ($\sigma = 1, 2, \dots, D-1$) and a longitudinal polarization ($\sigma = D$). For the longitudinal polarization one has $F_{il} = 0$ and the conditions (6.1) impose no restriction on the eigenvalues of the momentum k^D for that mode. For polarizations $\sigma = 1, 2, \dots, D-1$ the mode functions of the vector potential in the region $0 \leq z \leq a$ are presented in the form

$$A_{(\beta)l}(x) = C_{\beta\epsilon_{(\sigma)l}} \sin(k^D z) e^{-ik_j x_j^j}, \quad A_{(\beta)D} = 0, \quad (6.2)$$

with the eigenvalues of the momentum k^D determined by the boundary condition at $z = a$:

$$k^D = \frac{\pi n}{a}, \quad n = 1, 2, \dots \quad (6.3)$$

The normalization constant is determined from the condition (2.21) and coincides with (2.22). Note that in this case $n \neq 0$ and the zero mode is absent. The mode functions for the longitudinal polarization ($\sigma = D$) are given by

$$A_{(\beta)l} = -\frac{k_l k^D}{\lambda^2} C_{\beta} e^{-ik_{\mu} x^{\mu}}, \quad A_{(\beta)D} = C_{\beta} e^{-ik_{\mu} x^{\mu}}. \quad (6.4)$$

For these modes the components $F_{(\beta)il}$ of the field tensor vanish and they obey the boundary condition for $-\infty < k^D < +\infty$. The longitudinal mode is free to propagate in the region $-\infty < z < +\infty$ and in the normalization condition (2.21) the integration over z goes over that region. For the normalization constant we get

$$|C_{\beta}|^2 = \frac{\lambda^2}{(2\pi)^{D-1} m^2 \omega}, \quad \sigma = D. \quad (6.5)$$

The mode functions (6.4) coincide with the corresponding modes in the boundary-free problem with $-\infty < z < +\infty$. The Casimir contributions to the two-point functions and VEVs are obtained by subtracting from the total VEVs the parts corresponding to the boundary-free geometry. Thus, the longitudinal modes $\sigma = D$ will not contribute to the Casimir parts and in the discussion below we present the contributions in the expectation values corresponding to the transverse modes (polarizations $\sigma = 1, 2, \dots, D-1$).

6.2 Two-point functions

The contribution of the transverse modes to the expectation values will be denoted by $\langle \dots \rangle_{\text{tr}}$. For the components of the two-point function $\langle A_{\mu} A'_{\nu} \rangle_{\text{tr}}$ with $\mu = D$ or $\nu = D$ we have $\langle A_D A'_{\nu} \rangle_{\text{tr}} = \langle A_{\mu} A'_D \rangle_{\text{tr}} = 0$. For the evaluation of the VEVs of the fields squared and energy-momentum tensor one needs the expectation values $\langle A_l A'_p \rangle_{\text{tr}}$ in the coincidence limit $x' \rightarrow x$. In that limit they are diagonal and from the problem symmetry $\langle A_0 A^0 \rangle_{\text{tr}} = \dots = \langle A_{D-1} A^{D-1} \rangle_{\text{tr}}$. Hence, it suffices to consider the two-point function $\langle A_l A'^l \rangle_{\text{tr}}$. By using the modes (6.2) one obtains

$$\langle A_l A'^l \rangle_{\text{tr}} = (1 - D) B(x, x'), \quad (6.6)$$

with the function $B(x, x')$ defined by (3.4) and presented in the form (3.7).

The two-point functions of the field tensor are also expressed in terms of the function $B(x, x')$:

$$\begin{aligned} \langle F_{ik} F'_{lp} \rangle_{\text{tr}} &= 2 (g_{[ip} \partial_{k]} \partial'_l - g_{[il} \partial_{k]} \partial'_p) B(x, x'), \\ \langle F_{Dk} F'_{lp} \rangle_{\text{tr}} &= 2 g_{k[l} \partial'_{p]} \partial_D B(x, x'), \\ \langle F_{Dl} F'^l_D \rangle_{\text{tr}} &= (1 - D) \partial_D \partial'_D B(x, x'). \end{aligned} \quad (6.7)$$

By using the expression (3.7) we get the representation

$$\langle F_{\mu\nu} F'_{\rho\sigma} \rangle_{\text{tr}} = \frac{4m^{D+1}}{(2\pi)^{\frac{D-1}{2}}} \sum_{j=\mp 1} \sum_{n=-\infty}^{\infty} j G_{\mu\nu\rho\sigma}^{(j,n)}(x, x'), \quad (6.8)$$

where $G_{iklp}^{(j,n)}(x, x') = F_{iklp}^{(j,n)}(x, x')$ and $G_{Dklp}^{(j,n)}(x, x') = F_{Dklp}^{(j,n)}(x, x')$ with the components $F_{\mu\nu\rho\sigma}^{(j,n)}(x, x')$ from (3.24). The components with $\mu = \rho = D$, required in the evaluation of the VEVs in the coincidence limit are obtained from the two-point function $\langle F_{Dl} F_D^{l'} \rangle_{\text{tr}}$ and for it we have

$$G_{DlD}^{(j,n)\dots l}(x, x') = j \frac{D-1}{2} \left[m^2 (2na - z_j)^2 f_{\frac{D+3}{2}}(mb_{j,n}(x, x')) - f_{\frac{D+1}{2}}(mb_{j,n}(x, x')) \right]. \quad (6.9)$$

6.3 The Casimir densities

The expectation values of the physical characteristics for the vacuum state are obtained from the two-point functions in the limit $x' \rightarrow x$. For points away from boundaries the renormalization is reduced to the subtraction of the part in the two-point functions with $n = 0$ and $j = -1$. That part presents the contribution corresponding to the geometry without boundaries. As it has been discussed above, the longitudinal mode does not contribute to the subtracted (renormalized) VEVs and they will be denoted by $\langle \dots \rangle$ (omitting the subscript tr).

We start with the VEV $\langle A_\mu A_\nu \rangle$. One has $\langle A_D A_\nu \rangle = 0$ and

$$\langle A_i A_l \rangle = 2g_{il} \frac{(D-1)m^{D-1}}{(2\pi)^{\frac{D-1}{2}} D} \left[-2 \sum_{n=1}^{\infty} f_{\frac{D-1}{2}}(2nma) + \sum_{n=-\infty}^{+\infty} f_{\frac{D-1}{2}}(2mz_n) \right]. \quad (6.10)$$

Note that unlike to the case of the boundary condition (2.5), the VEV $\langle A_i A_l \rangle$ is finite in the zero-mass limit. Next we consider the condensate $\langle F_{\mu\nu} F^{\mu\nu} \rangle$. From (6.8) one obtains

$$\begin{aligned} \langle F_{\mu\nu} F^{\mu\nu} \rangle &= \frac{4(1-D)m^{D+1}}{(2\pi)^{\frac{D-1}{2}}} \left\{ 2 \sum_{n=1}^{\infty} f_{\frac{D-1}{2}}(2nma) \right. \\ &\quad \left. + \sum_{n=-\infty}^{\infty} \left[2D f_{\frac{D+1}{2}}(2mz_n) + f_{\frac{D-1}{2}}(2mz_n) \right] \right\}. \end{aligned} \quad (6.11)$$

The condensate is negative for $D \geq 2$ and vanishes for $D = 1$. Combining this with the expectation value (6.10), we get the VEV of the Lagrangian density:

$$\langle L(A_\mu) \rangle = \frac{(D-1)m^{D+1}}{(2\pi)^{\frac{D+1}{2}}} \sum_{n=-\infty}^{\infty} \left[D f_{\frac{D+1}{2}}(2mz_n) + f_{\frac{D-1}{2}}(2mz_n) \right]. \quad (6.12)$$

This VEV will be used in the evaluation of the energy-momentum tensor.

The VEVs of the electric and magnetic field squares are obtained by using the formulas (4.1) and (4.9). They are given by the expressions

$$\begin{aligned} \langle E^2 \rangle &= \frac{2(D-1)m^{D+1}}{(2\pi)^{\frac{D-1}{2}} D} \left\{ 2 \sum_{n=1}^{\infty} \left[f_{\frac{D-1}{2}}(2nma) - D f_{\frac{D+1}{2}}(2nma) \right] \right. \\ &\quad \left. + \sum_{n=-\infty}^{\infty} \left[3D f_{\frac{D+1}{2}}(2mz_n) + f_{\frac{D-1}{2}}(2mz_n) \right] \right\}, \end{aligned} \quad (6.13)$$

and

$$\begin{aligned} \langle B^2 \rangle = & \frac{2(1-D)m^{D+1}}{(2\pi)^{\frac{D-1}{2}}} \left\{ 2 \sum_{n=1}^{\infty} \left[f_{\frac{D+1}{2}}(2nma) + \frac{D-1}{D} f_{\frac{D-1}{2}}(2nma) \right] \right. \\ & \left. + \sum_{n=-\infty}^{\infty} \left[(2D-3) f_{\frac{D+1}{2}}(2mz_n) + \frac{D-1}{D} f_{\frac{D-1}{2}}(2mz_n) \right] \right\}. \end{aligned} \quad (6.14)$$

From the inequality (4.5) it follows that the VEV $\langle E^2 \rangle$ is positive for $D \geq 2$. The VEV of the magnetic field squared vanishes for $D = 1$ and is negative in spatial dimensions $D \geq 2$.

The expressions for the energy density and parallel stresses read (no summation over l)

$$\begin{aligned} \langle T_l^l \rangle = & \frac{(1-D)m^{D+1}}{(2\pi)^{\frac{D+1}{2}}} \left\{ 2 \sum_{n=1}^{\infty} f_{\frac{D+1}{2}}(2nma) \right. \\ & \left. + \sum_{n=-\infty}^{\infty} \left[(D-3) f_{\frac{D+1}{2}}(2mz_n) + \frac{D-2}{D} f_{\frac{D-1}{2}}(2mz_n) \right] \right\}. \end{aligned} \quad (6.15)$$

The vacuum energy density is negative for $D \geq 3$ and positive for $D = 2$. The normal stress is presented as

$$\langle T_D^D \rangle = \frac{2(D-1)m^{D+1}}{(2\pi)^{\frac{D+1}{2}}} \sum_{n=1}^{\infty} \left[D f_{\frac{D+1}{2}}(2nma) + f_{\frac{D-1}{2}}(2nma) \right]. \quad (6.16)$$

The VEV of the energy-momentum tensor vanishes for $D = 1$. As expected from the conservation equation for the energy-momentum tensor, the distribution of the normal stress in the region between the plates is uniform. For the Casimir pressure on the plates we have $p_C = -\langle T_D^D \rangle$ and the Casimir forces are attractive. Note that we have a simple relation between the Casimir forces for PMC and PEC boundary conditions:

$$\frac{\langle T_D^D \rangle_{\text{PMC}}}{\langle T_D^D \rangle_{\text{PEC}}} = \frac{D}{D-1}. \quad (6.17)$$

Note that the expression on the right-hand side of (6.17) is the ratio of the number of independent polarizations of the vector field influenced by PMC and PEC boundary conditions. For the trace of the energy-momentum tensor we obtain

$$\begin{aligned} \langle T_l^l \rangle = & \frac{(1-D)m^{D+1}}{(2\pi)^{\frac{D+1}{2}}} \left\{ -2 \sum_{n=1}^{\infty} f_{\frac{D-1}{2}}(2nma) \right. \\ & \left. + \sum_{n=-\infty}^{\infty} \left[D(D-3) f_{\frac{D+1}{2}}(2mz_n) + (D-2) f_{\frac{D-1}{2}}(2mz_n) \right] \right\}. \end{aligned} \quad (6.18)$$

For $D = 3$ it vanishes in the massless limit and the trace anomaly for PEC conditions is absent.

The vacuum densities in the problem with a single plate $z = 0$ are given by the terms $n = 0$ in the expressions given above. For the VEVs of the electric and magnetic field squares one has

$$\begin{aligned} \langle E^2 \rangle_1 = & \frac{2(D-1)m^{D+1}}{(2\pi)^{\frac{D-1}{2}} D} \left[3D f_{\frac{D+1}{2}}(2m|z|) + f_{\frac{D-1}{2}}(2m|z|) \right], \\ \langle B^2 \rangle_1 = & \frac{2(1-D)m^{D+1}}{(2\pi)^{\frac{D-1}{2}}} \left[(2D-3) f_{\frac{D+1}{2}}(2m|z|) + \frac{D-1}{D} f_{\frac{D-1}{2}}(2m|z|) \right]. \end{aligned} \quad (6.19)$$

They vanish for $D = 1$. The VEV of the electric field squared is positive and the VEV of the magnetic field squared is negative for $D \geq 2$. The vacuum energy density and the parallel stresses are expressed

as (no summation over l)

$$\langle T_l^l \rangle_1 = \frac{(1-D)m^{D+1}}{(2\pi)^{\frac{D+1}{2}}} \left[(D-3) f_{\frac{D+1}{2}}(2m|z|) + \frac{D-2}{D} f_{\frac{D-1}{2}}(2m|z|) \right], \quad (6.20)$$

and the normal stress vanishes. As seen, the Casimir densities for the PEC conditions vanish for spatial dimension $D = 1$. We could expect that result, by taking into account that for $D = 1$ the only polarization mode is longitudinal and the PEC conditions do not affect that mode.

Figure 5 presents the dependence of the electric ($U = E$, full curves) and magnetic ($U = B$, dashed curves) field squares (in units m^{D+1}) on z/a . The graphs are plotted for $ma = 0.75, 1, 1.25, 1.5$ (the ratio $|\langle U^2 \rangle|/m^{D+1}$ decreases with increasing m). The analysis for the VEV $\langle E^2 \rangle$ given above shows that for PEC boundary conditions the Casimir-Polder force acting on a polarizable microparticle is attractive with respect to the nearest plate for spatial dimensions $D \geq 2$. The vacuum energy density, measured

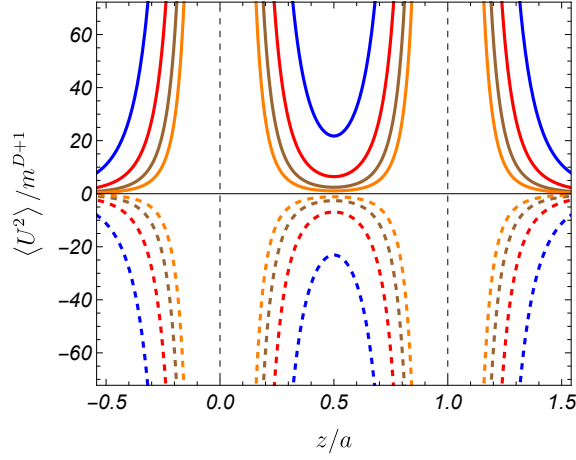


Figure 5: VEVs of the electric and magnetic field squares (in units m^{D+1}) for the Proca field with PEC boundary conditions in 3-dimensional space as functions of z/a . For the parameter ma the values $ma = 0.75, 1, 1.25, 1.5$ are taken (the ratio $|\langle U^2 \rangle|/m^{D+1}$ is a decreasing function of ma).

in units m^{D+1} and given by (6.15) and (6.20) with $l = 0$, is plotted in figure 6 as a function of z/a for the same values $ma = 0.75, 1, 1.25, 1.5$. The modulus of the ratio $\langle T_0^0 \rangle/m^{D+1}$ decreases with increasing ma . The behavior of the Casimir pressure p_C for a vector field with PEC conditions on the plates, as a function of ma , directly follows from figure 4 by taking into account the relation (6.17).

In the massless limit the expressions for the VEVs of the electric and magnetic field squares in the region between the plates are simplified to

$$\begin{aligned} \langle E^2 \rangle_{m \rightarrow 0} &= \frac{(1-D)\Gamma(\frac{D+1}{2})}{(4\pi)^{\frac{D-1}{2}} a^{D+1}} \left[\zeta(D+1) - \sum_{n=-\infty}^{\infty} \frac{3/2}{|n - z/a|^{D+1}} \right], \\ \langle B^2 \rangle_{m \rightarrow 0} &= \frac{(1-D)\Gamma(\frac{D+1}{2})}{(4\pi)^{\frac{D-1}{2}} a^{D+1}} \left[\zeta(D+1) + \sum_{n=-\infty}^{\infty} \frac{D-3/2}{|n - z/a|^{D+1}} \right]. \end{aligned} \quad (6.21)$$

For the VEVs of the components of the energy-momentum tensor we get

$$\begin{aligned} \langle T_l^l \rangle_{m \rightarrow 0} &= \frac{(1-D)\Gamma(\frac{D+1}{2})}{(4\pi)^{\frac{D+1}{2}} a^{D+1}} \left[\zeta(D+1) + \sum_{n=-\infty}^{\infty} \frac{(D-3)/2}{|n - z/a|^{D+1}} \right], \\ \langle T_D^D \rangle_{m \rightarrow 0} &= \frac{D(D-1)\Gamma(\frac{D+1}{2})}{(4\pi)^{\frac{D+1}{2}} a^{D+1}} \zeta(D+1). \end{aligned} \quad (6.22)$$

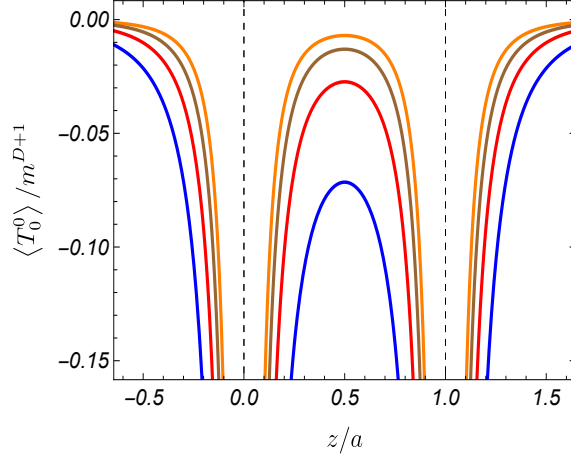


Figure 6: Vacuum energy density (in units of m^{D+1}) for a $D = 3$ massive vector field with PEC conditions versus z/a . The graphs are plotted for the values $ma = 0.75, 1, 1.25, 1.5$. The modulus of the ratio $\langle T_0^0 \rangle / m^{D+1}$ decreases with increasing ma .

The limiting VEVs (6.21) and (6.22) coincide with the corresponding expectation values for a massless vector field. They are obtained from the results in [29] for the AdS bulk in the limit of the infinite curvature radius. In the special case $D = 3$, from (6.22) we get the Casimir result $p_C = -\pi^2/(240a^4)$ for the vacuum pressure. In this case, the Casimir energy density is zero in the regions $z < 0$ and $z > a$ and its distribution in the region between the plates is uniform. Figure 7 presents the dependence of the Casimir energy density (in units of $1/a^{D+1}$) for a massless vector field with PEC boundary conditions on the ratio z/a in spatial dimensions $D = 3, 4, 5, 6$. The modulus of the combination $a^{D+1} \langle T_0^0 \rangle$ increases with increasing D .

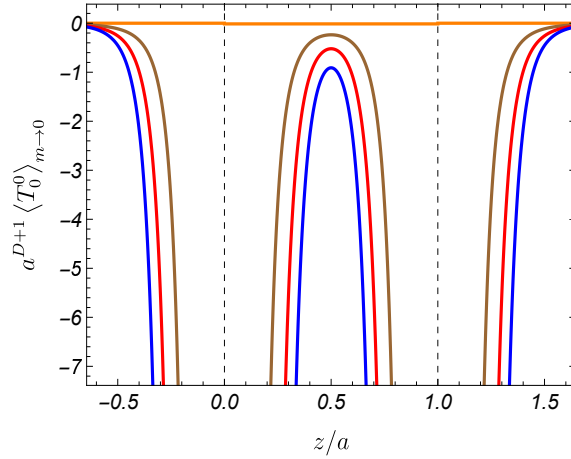


Figure 7: Vacuum energy density (in units $1/a^{D+1}$) as a function of z/a for a massless vector field with PEC boundary conditions. The graphs are plotted for the values of the spatial dimension $D = 3, 4, 5, 6$. The product $a^{D+1} |\langle T_0^0 \rangle|$ increases with increasing D .

As we have seen, an important difference between the two types of boundary conditions discussed above is that the PMC conditions constrain all the polarization states of the Proca field, whereas the longitudinal polarization modes are not influenced by PEC condition. As a consequence, for the first case, the regions separated by the reflecting surfaces (hyperplanes $z = 0$ and $z = a$ in the present problem) are causally independent and the local characteristics of the vacuum state in the given region do not depend on the physical conditions in other regions. For example, we can consider a problem involving a single,

finite-thickness PMC plate occupying the spatial region $0 \leq z \leq L$. In this geometry, the VEVs in the regions $z < 0$ and $z > L$ (the vacuum regions) will be expressed by the formulas given above for PMC conditions (with a replaced by L). The PEC interfaces are transparent to the longitudinal polarization modes of the Proca field, so the VEVs in separate regions are sensitive to the physical conditions in other regions. In this case, the longitudinal polarization modes will contribute to the Casimir densities. Examples for the total Casimir energy and forces in the problem of two parallel plates of finite thickness have been studied in [15, 16, 17, 20].

7 Conclusion

We have studied the Casimir effect for a massive vector field in a general number of spatial dimensions. The geometry of two parallel plates is considered with two types of boundary conditions. The first one, referred to as PMC condition, is a higher dimensional generalization of the boundary conditions used in bag models of hadrons to confine the gluon fields inside a finite volume and the second one (PEC condition) generalizes the boundary condition imposed on the surface of perfect conductors in Maxwell electrodynamics. The massive vector field in $(D + 1)$ -dimensional spacetime has D independent polarization states: $D - 1$ states with transversal polarization and one state of longitudinal polarization. The PMC conditions constrain all the polarization states, whereas the PEC conditions do not act on the longitudinal polarization. Due to this feature, the massless limit of the vacuum local characteristics is significantly different for those boundary conditions.

In the problem under consideration, all the properties of the vacuum state are encoded in two-point functions. As such we have taken the positive frequency Wightman functions for the vector potential and the field tensor. The evaluation procedure is based on the direct summation of the corresponding mode sums over a complete set of mode functions obeying the boundary conditions. In the region between the plates, the mode functions for the PMC conditions are given by (2.15) and (2.19) with the eigenvalues for the normal component of the wave vector given by (2.18) (excluding the mode $n = 0$ for the longitudinal polarization). The two-point function for the vector potential is expressed as (3.10), where the separate terms in the summation are defined by (3.11). It is decomposed into three contributions (3.13), corresponding to the boundary-free geometry, the part induced by a single boundary, and the contribution generated by the second boundary. The massless limit of the two-point function for the vector potential is singular: it diverges like $1/m^2$ (see (3.15)). The two-point function for the field tensor in the problem with PMC conditions is given by (3.23) and (3.24) and its massless limit is finite (see (3.25)).

The Casimir densities are obtained from the two-point functions in the coincidence limit of the space-time arguments. For points outside the plates, the divergences are contained in the parts corresponding to the boundary-free problem. In our representations of the two-point functions those parts are explicitly separated and the renormalization is reduced to the subtraction of them. As important local characteristics of the vacuum state, we have considered the expectation values of the electric and magnetic field squares, of the energy-momentum tensor, and the vector field condensate. The corresponding VEVs in the geometry of a single plate are obtained in the limit $a \rightarrow \infty$. The single plate contributions dominate in the total VEVs for points near the plates. For PMC boundary conditions the VEV of the electric field squared is negative. The corresponding Casimir-Polder forces, acting on a polarizable microparticle, are repulsive with respect to the nearest plate. The VEV of the magnetic field squared vanishes for $D = 1$ and is positive in dimensions $D \geq 2$. The vacuum energy density in the region between the plates is negative for $D = 1, 2$ and positive for $D \geq 3$. It is uniformly distributed in the spatial dimension $D = 2$. The vacuum energy density in the regions $z < 0$ and $z > a$ is negative for $D = 1$ and positive for $D \geq 3$. In those regions, the vacuum energy-momentum tensor vanishes for $D = 2$. The Casimir forces are attractive for all separations between the plates. For a massive field, they exponentially decay at large separations. We have also provided the expressions for the VEVs in the massless limit. The VEV of the energy-momentum tensor in that limit is traceless for $D = 1, 2$ and has a nonzero trace for $D \geq 3$.

To compare the VEVs in the zero-mass limit of the Proca field, obeying PMC boundary conditions, with the corresponding expectation values for a massless vector field, we have separately studied the two-point functions and the Casimir densities in the massless case. The VEVs of the electric and magnetic field squares, as well as the condensate, are entirely determined by the two-point function of the field tensor. In the zero-mass limit, these VEVs coincide with those for a massless field. This is not the case for the VEV of the energy-momentum tensor which also receives the contribution from the two-point function of the vector potential. The longitudinal polarization is absent for a massless field, whereas its contribution to the vacuum energy-momentum tensor for the Proca field does not vanish in the zero-mass limit.

We have also considered the two-point functions and the Casimir densities for the Proca field with the PEC boundary conditions on the plates. These conditions do not constrain the mode with longitudinal polarization and the latter does not contribute to the Casimir parts in the VEVs. The transverse polarization modes are given by (6.2) with the quantized normal component of the wave vector (6.3). For the PEC conditions the two-point function of the vector potential is finite in the zero-mass limit. Consequently, the Casimir densities in the zero mass limit of the Proca field coincide with the corresponding VEVs for a massless vector field. The vacuum energy density is negative for $D \geq 3$, positive for $D = 2$, and vanishes for $D = 1$. The Casimir forces are attractive in spatial dimensions $D \geq 2$ and become zero for $D = 1$. For $D \geq 2$ the ratio of the Casimir forces for PMC and PEC boundary conditions is equal to the ratio of the number of independent polarizations influenced by those conditions. The VEV of the electric field squared for PEC conditions is positive for $D \geq 2$ and the corresponding Casimir-Polder forces are attractive with respect to the nearest plate.

Acknowledgments

The work was supported by the grants No. 21AG-1C047 and No. 24AA-1C025 of the Higher Education and Science Committee of the Ministry of Education, Science, Culture and Sport RA.

A Transformation of the function $A_j(x, x')$

In this Appendix we present the transformation of the two-point function (3.6). The summation over n in (3.6) is done by using the Abel-Plana formula

$$\sum_{n=0}^{\infty} f(n) = \int_0^{\infty} dy f(y) + i \int_0^{\infty} dy \frac{f(iy) - f(-iy)}{e^{2\pi y} - 1}, \quad (\text{A.1})$$

with the function

$$f(y) = \frac{e^{-i\omega t}}{\omega} \cos(b_j y), \quad \omega = \sqrt{\omega_{\mathbf{k}}^2 + (\pi y/a)^2}, \quad \omega_{\mathbf{k}} = \sqrt{\mathbf{k}^2 + m^2}. \quad (\text{A.2})$$

For the series in (3.6) one has $b_j = |z + jz'|$. Assuming that $b_j + |\Delta t| < 2a$, one gets

$$\sum_{n=0}^{\infty} \frac{e^{-i\omega \Delta t}}{\omega} \cos(b_j k_D) = \frac{a}{\pi} \int_0^{\infty} du \cos(b_j u) \frac{e^{-i\sqrt{u^2 + \omega_{\mathbf{k}}^2} \Delta t}}{\sqrt{u^2 + \omega_{\mathbf{k}}^2}} + \frac{2a}{\pi} \int_{\omega_{\mathbf{k}}}^{\infty} du \frac{\cosh\left(\sqrt{u^2 - \omega_{\mathbf{k}}^2} \Delta t\right)}{\sqrt{u^2 - \omega_{\mathbf{k}}^2} (e^{2au} - 1)} \cosh(b_j u). \quad (\text{A.3})$$

In the first integral we write $\cos(b_j u) = (e^{ib_j} + e^{-ib_j})/2$ and rotate the integration contour in the complex u -plane by the angle $\pi/2$ for the part with e^{ib_j} and by the angle $-\pi/2$ for the part with e^{-ib_j} . In this way it can be seen that

$$\int_0^{\infty} du \cos(b_j u) \frac{e^{-i\sqrt{u^2 + \omega_{\mathbf{k}}^2} \Delta t}}{\sqrt{u^2 + \omega_{\mathbf{k}}^2}} = \int_{\omega_{\mathbf{k}}}^{\infty} du \frac{\cosh\left(\sqrt{u^2 - \omega_{\mathbf{k}}^2} \Delta t\right)}{\sqrt{u^2 - \omega_{\mathbf{k}}^2}} e^{-b_j u}. \quad (\text{A.4})$$

By using this relation in (A.3) we obtain

$$\sum_{n=0}^{\infty} f(n) = \frac{a}{\pi} \int_{\omega_{\mathbf{k}}}^{\infty} du \frac{\cosh(\sqrt{u^2 - \omega_{\mathbf{k}}^2} \Delta t)}{\sqrt{u^2 - \omega_{\mathbf{k}}^2}} \left[e^{-b_j u} + \frac{2 \cosh(b_j u)}{e^{2au} - 1} \right]. \quad (\text{A.5})$$

This gives

$$A_j(x, x') = \frac{1}{\pi} \int \frac{d\mathbf{k}}{(2\pi)^{D-2}} \int_{\omega_{\mathbf{k}}}^{\infty} du \frac{\cosh(\sqrt{u^2 - \omega_{\mathbf{k}}^2} \Delta t)}{\sqrt{u^2 - \omega_{\mathbf{k}}^2}} \left[e^{-b_j u} + \frac{2 \cosh(b_j u)}{e^{2au} - 1} \right]. \quad (\text{A.6})$$

For the integration over the angular part of the vector \mathbf{k} , we introduce in (A.6) spherical coordinates in the momentum space with the polar axis along the vector $\Delta \mathbf{x}_{\parallel}$. The integral over the angles is expressed in terms of the Bessel function $J_{(D-3)/2}(k|\Delta \mathbf{x}_{\parallel}|)$, where $k = |\mathbf{k}|$. As the next step we introduce a new integration variable $w = \sqrt{u^2 - \omega_{\mathbf{k}}^2}$ and then pass to the polar coordinates in the plane (w, k) . The integral over the corresponding polar angle is evaluated by using the formula [32]

$$\int_0^1 dx x^{\nu+1} \frac{\cosh(b\sqrt{1-x^2})}{\sqrt{1-x^2}} J_{\nu}(cx) = \sqrt{\frac{\pi}{2}} c^{\nu} \frac{J_{\nu+1/2}(\sqrt{c^2-b^2})}{(c^2-b^2)^{\frac{2\nu+1}{4}}}. \quad (\text{A.7})$$

As a result, the representation

$$A_j(x, x') = \frac{(2\pi)^{1-\frac{D}{2}}}{(-\Delta x_l \Delta x^l)^{\frac{D-2}{4}}} \int_0^{\infty} dr r^{\frac{D}{2}-1} J_{\frac{D}{2}-1}(r\sqrt{-\Delta x_l \Delta x^l}) \frac{1}{u} \left[e^{-b_j u} + \frac{2 \cosh(b_j u)}{e^{2au} - 1} \right]_{u=\sqrt{r^2+m^2}} \quad (\text{A.8})$$

is obtained, where $\Delta x_l \Delta x^l = (\Delta t)^2 - |\Delta \mathbf{x}_{\parallel}|^2$. An alternative representation is obtained by using the relation

$$\frac{2 \cosh(b_j u)}{e^{2au} - 1} = \sum_{s=\pm 1} \sum_{n=1}^{\infty} e^{-(2na-sb_j)u}. \quad (\text{A.9})$$

With this expansion, the integral over r is evaluated by the formula [32]

$$\int_0^{\infty} dr r^{D/2} J_{\frac{D}{2}-1}(r\sqrt{-\Delta x_l \Delta x^l}) \frac{e^{-c\sqrt{r^2+m^2}}}{\sqrt{r^2+m^2}} = \sqrt{\frac{2}{\pi}} m^{D-1} (-\Delta x_l \Delta x^l)^{\frac{D-2}{4}} f_{\frac{D-1}{2}}(m\sqrt{c^2 - \Delta x_l \Delta x^l}), \quad (\text{A.10})$$

with the function (3.9). As a result, the representation

$$A_j(x, x') = \frac{2m^{D-1}}{(2\pi)^{\frac{D-1}{2}}} \sum_{n=-\infty}^{+\infty} f_{\frac{D-1}{2}}(m\sqrt{(2na-z-jz')^2 - \Delta x_l \Delta x^l}), \quad (\text{A.11})$$

is obtained.

References

- [1] V.M. Mostepanenko, N.N. Trunov, The Casimir Effect and Its Applications (Clarendon, Oxford, 1997).
- [2] K.A. Milton, The Casimir Effect: Physical Manifestation of Zero-Point Energy (World Scientific, Singapore, 2002).

- [3] M. Bordag, G.L. Klimchitskaya, U. Mohideen, V.M. Mostepanenko, *Advances in the Casimir Effect* (Oxford University Press, New York, 2009).
- [4] *Casimir Physics*, edited by D. Dalvit, P. Milonni, D. Roberts, F. da Rosa, *Lecture Notes in Physics* Vol. 834 (Springer-Verlag, Berlin, 2011).
- [5] A.A. Saharian, T.A. Vardanyan, Casimir densities for a plate in de Sitter spacetime, *Classical Quantum Gravity* **26**, 195004 (2009).
- [6] E. Elizalde, A.A. Saharian, T.A. Vardanyan, Casimir effect for parallel plates in de Sitter spacetime, *Phys. Rev. D* **81**, 124003 (2010).
- [7] K.A. Milton, A.A. Saharian, Casimir densities for a spherical boundary in de Sitter spacetime, *Phys. Rev. D* **85**, 064005 (2012).
- [8] L.-C. Tu, J. Luo, G.T. Gillies, The mass of the photon, *Rep. Prog. Phys.* **68**, 77 (2005).
- [9] A.S. Goldhaber, M.M. Nieto, Photon and graviton mass limits, *Rev. Mod. Phys.* **82**, 939 (2010).
- [10] A. Proca, Sur la théorie ondulatoire des électrons positifs et négatifs, *J. Phys. Radium* **7**, 347 (1936).
- [11] E.C.G. Stueckelberg, Interaction energy in electrodynamics and in the field theory of nuclear forces, *Helv. Phys. Acta* **11**, 225 (1938).
- [12] E.C.G. Stueckelberg, Interaction forces in electrodynamics and in the field theory of nuclear forces, *Helv. Phys. Acta* **11**, 299 (1938).
- [13] H. Ruegg, M. Ruiz-Altaba, The Stueckelberg field, *Int. J. Mod. Phys. A* **19**, 3265 (2004).
- [14] P.C.W. Davies, S.D. Unwin, Quantum vacuum energy and the masslessness of the photon, *Phys. Lett. B* **98**, 274 (1981).
- [15] G. Barton, The Casimir effect with finite mass photons, *Annals Phys.* **162**, 231 (1985).
- [16] L.P. Teo, Casimir effect of massive vector fields, *Phys. Rev. D* **82**, 105002 (2010).
- [17] L.P. Teo, Zero and finite temperature Casimir effect of massive vector field between real metals, *J. Math. Phys.* **53**, 102302 (2012).
- [18] L.P. Teo, The Casimir interaction of a massive vector field between concentric spherical bodies, *Phys. Lett. B* **696**, 529 (2011).
- [19] L. Mattioli, A.M. Frassino, O. Panella, Casimir-Polder interactions with massive photons: Implications for BSM physics, *Phys. Rev. D* **100**, 116023 (2019).
- [20] A. Edery, V. Marachevsky, Compact dimensions and the Casimir Effect: The Proca Connection, *JHEP* **12** (2008) 035.
- [21] L.P. Teo, Casimir effect of electromagnetic field in Randall-Sundrum spacetime, *JHEP* **10** (2010) 019.
- [22] A. Belokogne, A. Folacci, Stueckelberg massive electromagnetism in curved spacetime: Hadamard renormalization of the stress-energy tensor and the Casimir effect, *Phys. Rev. D* **93**, 044063 (2016).
- [23] R.S. Decca, D. López, E. Fischbach, G.L. Klimchitskaya, D.E. Krause, V.M. Mostepanenko, Novel constraints on light elementary particles and extra-dimensional physics from the Casimir effect, *Eur. Phys. J. C* **51**, 963 (2007).

- [24] G.L. Klimchitskaya, V.M. Mostepanenko, Constraints on axionlike particles and non-Newtonian gravity from measuring the difference of Casimir forces. *Phys. Rev. D* **95**, 123013 (2017).
- [25] G.L. Klimchitskaya, Constraints on theoretical predictions beyond the Standard Model from the Casimir effect and some other tabletop physics, *Universe* **7**, 47 (2021).
- [26] A.E.R. López, V. Giannini, Casimir nanoparticle levitation in vacuum with broadband perfect magnetic conductor metamaterials, arXiv:2210.12094.
- [27] N.D. Birrell, P.C.W. Davies, *Quantum Fields in Curved Space* (Cambridge University Press, Cambridge, England, 1982).
- [28] A. Edery, V. Marachevsky, Perfect magnetic conductor Casimir piston in $d+1$ dimensions, *Phys. Rev. D* **78**, 025021 (2008).
- [29] A.A. Saharian, A.S. Kotanjyan, H.G. Sargsyan, Electromagnetic field correlators and the Casimir effect for planar boundaries in AdS spacetime with application in braneworlds, *Phys. Rev. D* **102**, 105014 (2020).
- [30] A.A. Saharian, A.S. Kotanjyan, H.A. Nersisyan, Electromagnetic two-point functions and Casimir densities for a conducting plate in de Sitter spacetime, *Phys. Lett. B* **728**, 141 (2014).
- [31] A.S. Kotanjyan, A.A. Saharian, H.A. Nersisyan, Electromagnetic Casimir effect for conducting plates in de Sitter spacetime, *Phys. Scr.* **90**, 065304 (2015).
- [32] A.P. Prudnikov, Yu.A. Brychkov, O.I. Marichev, *Integrals and Series* (Gordon and Breach, New York, 1986), Vol. 1,2.